Dynamics of expanding slug flow bubbles in non-Newtonian drilling fluids

A. H. Rabenjafimanantsoa, Rune W. Time, Thomas Paz

University of Stavanger, Norway

ABSTRACT

The motion of expanding slug bubbles in near vertical flows is investigated for non-Newtonian liquids simulating drilling fluids. It is a challenge both from engineering points of view and for theoretical-numerical simulations of slug flow to know how the gas bubbles trailing a Taylor bubble will spread along the tail of the bubble. A very important industrial example is gas-kicks during drilling of petroleum wells. The influence of main parameters including shear conditions and turbulence intensity at the rear of the bubble, as well as the ability of the fluid to keep the trailing bubbles in suspension were investigated. The experiments were done using high speed camera and PIV technique in a 5 meter high pipe of 8 cm inner diameter. Comparisons were done between Newtonian and non-Newtonian fluids. Different initial pressures in the slug bubbles were used to investigate transient effects.

INTRODUCTION

Different flow patterns occur through a vertical conduit during simultaneous flowing of liquid and gas. One of these flow patterns is slug flow. Such flow pattern is characterized by an alternate flowing of large bubbles, known as Taylor bubbles, separated by liquid slugs. This type of flow is identified in engineering applications, such as gas kick in oil and gas wells and geothermal fermentation, among others[1,2]. The slug can in some situation give efficient mixing by taking profit from the wake region.

TAYLOR BUBBLE

Following the description of Das *et al.*[3], a Taylor bubble in a circular pipe is symmetric about the vertical axis and comprises two regions, see figure 1. As seen in

Figure 1: Photograph of a Taylor Bubble.

figure 1 the upper part is the nose region and the lower part the tail region. The shape of the nose region is spherical while that of the tail region is cylindrical. The

flowing liquid around the bubble forms a falling film under gravity. The end of the bubble is separated from this film and creates a liquid wake. This is attached to the bubble rising and the pipe wall. This film creates a vortex as it merges to the surrounding liquid below,i.e at the rear of the bubble.
An universal correlation for the rise velocity of long gas bubbles in round pipe has been compiled[4]. It was found that:

$$U = K\sqrt{gD} \tag{1}$$

where,

U	is bubble velocity
K	is an empirical value about 0.351,
D	is pipe diameter, and
g	is acceleration due to gravity

This equation has been mentioned[4] to be a result of a large amount of compiled data by Dumitrescu in 1943 and further investigated by several authors. The goals of this work was to compare effects on Taylor bubbles in Newtonian versus non-Newtonian systems, as well as to determine the dynamics of quickly expanding bubbles.

EXPERIMENTAL

Experimental facility

The study was performed in the experimental setup schematized in figure 2. The facility consists mainly by an acrylic cylindrical pipe of 3.6 m height, H_1 and 8 mm internal diameter. The top of the pipe is made opened to the atmosphere. Another tube, H_3 is connected beneath the main column. A ball valve, H_2 is attached between these two pipes to facilitate the launch of a Taylor bubble. Another pipe L is further connected to the setup in order to make drainage easy during change of different fluid systems. Four differential pressure stations (P_0, P_1, P_2, P_3), as seen in figure 2 were mounted to the pipe. They were located at 1m apart from each other except from P_0 which was situated at 9cm

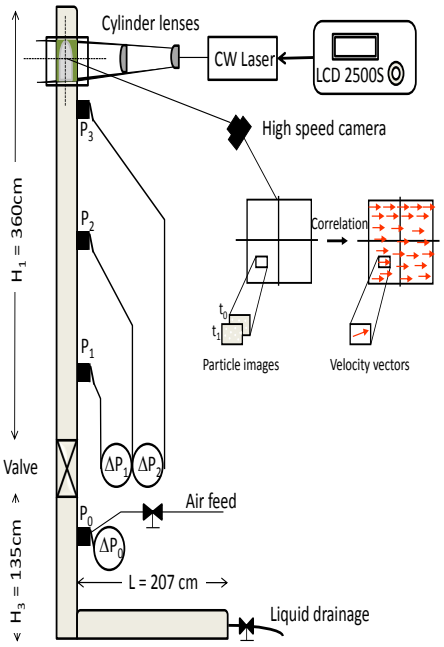

Figure 2: Schematic representation of the bubble transport system.

beneath the valve. A T-joint is connected to this station for air injection. The volume of bubble is controlled by closing the valve. Air is then injected to substitute approximately 700mL of drained liquid. The section below the valve can be pressurized in order to create initial conditions where a bubble expands more than if just starting to rise in stagnant liquid.

Differential pressures

ΔP_1 measures the pressure difference between the pressure stations P_2 and P_1, while ΔP_2 measures the pressure difference between the pressure stations P_3 and P_2. ΔP_0 measures the pressure at P_0 relative to the atmosphere. When a bubble passes the pressure stations, the differential pressures drops instantly. The bubble velocity can then be determined from the time of its passage between the differential pressure stations. The distance between two stations is, as mentioned set to $\Delta H = 1$m.

From the ΔP signals the bubble velocity and length could be determined since

the distance between the ΔP locations are known. When the signal drops quickly, the bubble nose passes the pressure stations, as illustrated in figure 3. Δt is the time difference between t_2 and t_1 which are relative to ΔP_2 and ΔP_1 locations.

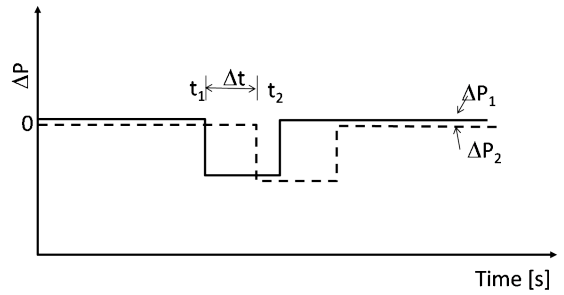

Figure 3: Illustration of the ΔP signals when the bubble nose passes two pressure locations.

LabView package was designed for the recording of the ΔP's. The scan rate was set to 250Hz. The visual test section was located at approximately 50 cm from the top of the tube. This was chosen to assure that the flow is well established.

The analysis of the experimental results is aimed at describing the detailed features of the flow using both Newtonian and non-Newtonian fluids.

Fluid rheology

Two different concentrations of polyanionic cellulose, PAC regular obtained from MI-Swaco, were used: 200 and 400 ppm PAC dissolved in water. A dispermix - stator on struts and foot bearing, type Shaft MD-LDT 1 connected to an Ystral motor from Maschinenbau + processtechnik was used for the preparation of the solution before pouring to the tube. The rheological measurements were taken using a Physica UDS 200 rheometer with cone plate configuration MK 24 (75 mm, 1^o). The two samples were measured at 20^oC with increasing shear rate to the maximum ($1022\ s^{-1}$) and decreasing again to the minimum ($1.5s^{-1}$). This was chosen to see any hysteresis effect.

The viscosity measurements were taken after the tests have been run. The viscosity of the fluids used is presented in figure 4.

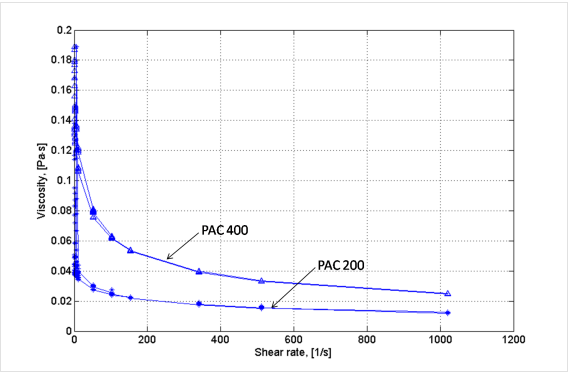

Figure 4: Viscosity versus shear rate at 20^oC of the 200 and 400 ppm concentrations of PAC dissolved in water.

For each solution, the focus was on Taylor bubble with a volume of approximately 700 mL air, as mentioned earlier. This is considered to be a sufficient length and that the liquid falling film flowing around the bubbles has developed.

Image analysis

The PIV technique is described by Rabenjafimanantsoa *et al.*[6] but we recall it here for brevity. The PIV system includes a Suwtech continuous wave (CW) diode laser giving a beam with 532nm wavelength. The beam is collimated into a 1mm thick and 5cm wide, nearly parallel "light sheet", using two cylinder lenses. The beam energy is adjustable up to 200mW using a Photop LDC-2500S power supply. A high speed camera (MiniVis e2, 512x512 pixels, 2500 fps) was computer controlled using the software program MotionBlitz from Mikrotron, to record series of pictures. Acquired images from the MiniVis camera were imported in DynamicStudio[7] version 2.10 from DantecDynamics for postprocessing. The processing unit performs picture analysis to determine particle velocity based on a two-dimensional cross correlation technique. In addition, light emitting diodes (LEDs) were also setup in some situ-

ations. In this work, the interrogation windows was 32x32 pixels with 50% overlap.

MatPIV[8] version 1.6.1 was also used in postprocessing the images. The detail performance of this Matlab toolbox is explained in Rabenjafimanantsoa[9], but briefly recalled here for clarity. Pairs of images were used for calculation of velocities in the (x,y)-plane. The velocities were obtained by a four step cross correlation calculation (64x64, 32x32, 16x16, 16x16, 50% overlap). This is achieved using the 'multin' option (multiple pass analysis) which calculates the PIV vectors using 4 iterations starting from 64x64 windows and finishing with 16x16. The scale factor which is the conversion from pixels to the 'real world' co-ordinates was obtained from DynamicStudio.

EXPERIMENTAL RESULTS

Figure 5 shows the ΔP signals from water flow when the bubble passes through the pressure stations (top) and the pressure applied during the release. This was clearly illustrated in figure 3. The plot in figure 5 shows a "running time average" of original pressure recordings at 250 Hz sampling rate, together with error bands given by one standard deviation. For the plot is used the average of 20 recordings, centered within each time segment. As seen in figure 5 (top) and referring to figure 3, the ΔP's are zero and the ΔP_0 is measured to be 650mbar. At approximately 3.5s abrupt increases in ΔP_1 and ΔP_2 is observed. At the same time ΔP_0 decreases to approximately 325mbar. This is the time of release of the bubble. The observed permanent loss is due to two factors; the release from the pressurized section below the valve, and the gas trapped and released as the Taylor bubble. In figure 5 (top), two datatips are displayed, $\Delta P_1(6.764)$ and $\Delta P_2(10.12)$. They show the respective time and ΔP when the bubble nose has traveled 1m. At these times, the ΔP's drop abruptly indicating that the

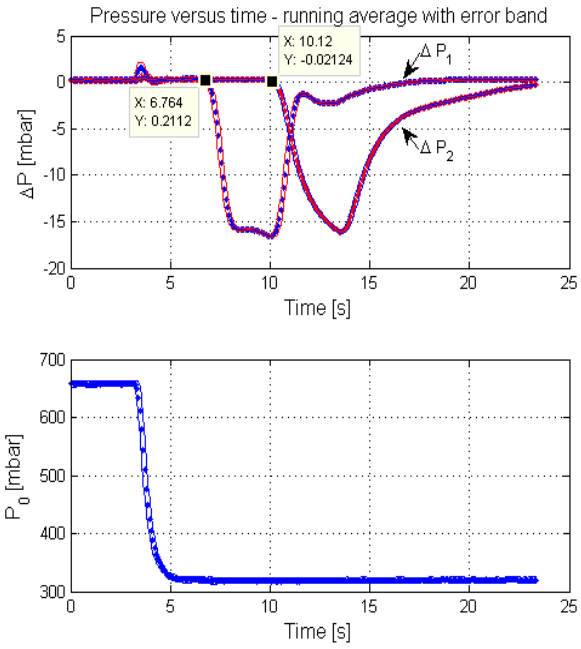

Figure 5: ΔP signals in water flows showing the passage of the bubble between two pressure stations (top) and the pressure applied to the bubble during release (bottom).

bubble nose has passed the pressure stations. Knowing that the stations are located at 1m apart from each other, it can be calculated that the bubble velocity is equal to be 0.295 m/s. In addition, applying the equation (1) the bubble velocity is calculated to be 0.31 m/s.

The flow field ahead of the Taylor bubble nose were captured by applying the PIV technique. The averaged vector fields as seen in figure 6 are superimposed with the image for a better visualization. This was processed using the DynamicStudio software. From figure 6 the averaged velocity profiles in the vertical direction shows the Newtonian liquid flow in front of the bubble. The liquid is pushed upwards and the liquid which is flowing around the bubble forms a falling film. The averaged velocity fields presented here were determined from 20 instantaneous velocity fields.

The same region was also processed using MatPIV. The time between two con-

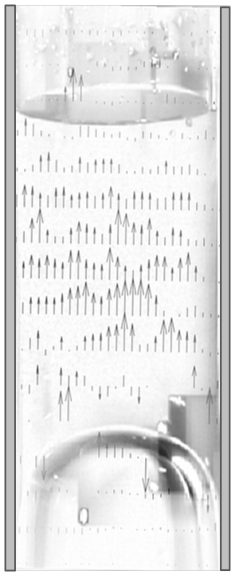

Figure 6: Superposition of the average flow field and a bubble image around the nose region of the Taylor bubble in water flows.

secutive images captured by the high speed camera was 0.04s. The images was inverted in order for MatPIV to work. 100 μm of glass beads were used as seeding particles. Figure 7 shows a superposition of a bubble image and an instantaneous velocity profile around the nose region using 400 ppm PAC. It can be seen from figure 7 that as the Taylor bubble moves upwards, the 400 ppm PAC solution in front of the bubble is pushed forward and away from the center. The velocity vectors are showing the intensity and the direction of the flow. This situation leads to the falling liquid thin film between the pipe wall and the bubble. The bubble shape in Newtonian is different from that of non-Newtonian fluids at the bottom region of the bubble. High speed images used for PIV showing this difference is represented in figure 8. For the PAC flows as seen in figure 8 (left) the bottom surface is more or less stable as the bubble rises. As the viscosity was increased, the trailing edge becomes more flat. This was also observed by other authors[1,2] in Carboxymethylcellulose (CMC) and Polyacrylamide (PAA) flows.

A sequence of images from different

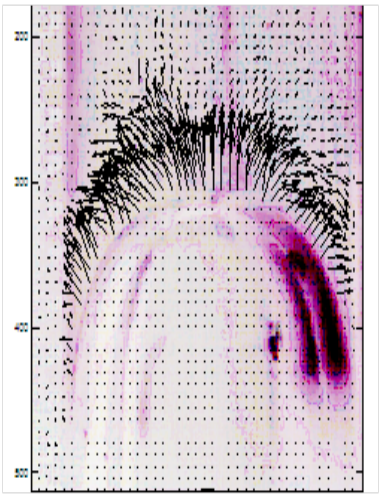

Figure 7: Instantaneous velocity profile superimposed with the bubble image around the nose region in PAC 400 flows. The image is inverted for clarity.

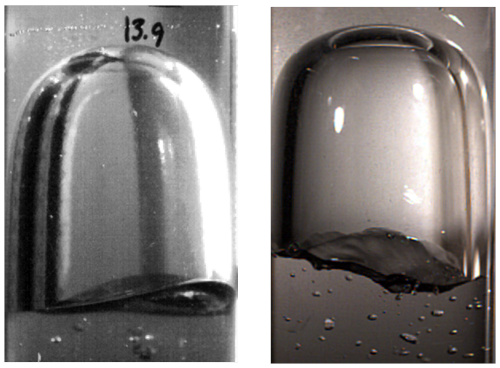

Figure 8: Bottom region high speed images for 400 ppm PAC (left) and water flows.

frames is presented in figure 9. It is from the recorded frame 3077 (left) to frame 3097 (right) in figure 9, possible to observe capillary wave. These waves appeared some time after the coalescence of the bubble with the surrounding liquid. From the high speed images the time between the frames 3077 to 3097 was 80ms corresponding to a 3.6cm film length. This will give a wave velocity of 45cm/s. A visualization box is needed to measure the thickness as a function of fluid viscosity as well as its dynamics.

Small bubbles are present in the wake and tail several meters behind the Taylor bubble. This is reflected both in the

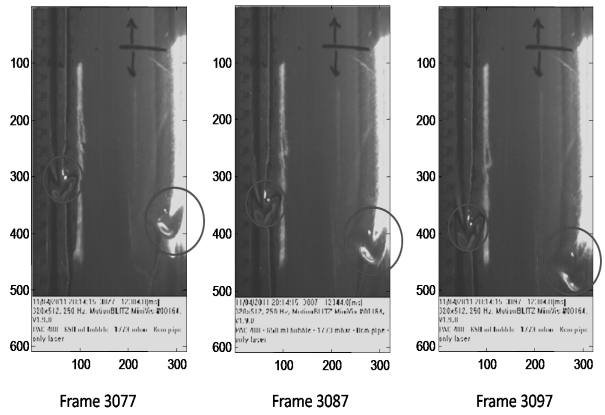

Figure 9: Sequence of frames showing capillary waves (encircled) in 400 ppm PAC flow. The time between frames is 40ms.

high-speed images and in the ΔP measurements. These small bubbles are formed due to the jet and the wake instability at the trailing edge of the Taylor bubble. Even for a very long pipe this pattern will be an integral part of the Taylor bubble regime, when its rise velocity exceeds a critical value determined by viscosity and surface tension.

Similar figures as illustrated in figure 3 and plotted in figure 5 (top) were expected both of 200 and 400 ppm PAC flows. However, during the experimental runs, electrical noise and / or grounding problems in the experimental hall impacted strongly on the pressure readings making the logged values improbable. As an example, 200 ppm PAC dissolved in water is presented in figure 10 using the same averaging method as mentioned earlier. It can be seen from figure 10 (top) that ΔP_1 is essentially zero until at approximately 13s where the bubble was released. A sudden increase is observed followed by a decrease to reach a minimum. At the same time ΔP_2 starts to decrease indicating that the bubble has passed the ΔP_2 location. The ΔP_2 which was expected to follow the same trend as in figure 5 (top) might have been exposed to erroneous signals, as mentioned, and therefore has too small negative amplitude. The

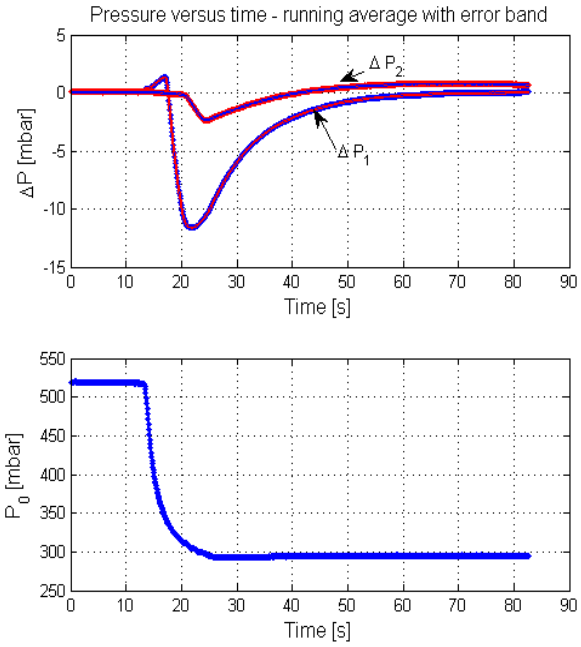

Figure 10: ΔP as a function of time (top) and the pressure applied to the bubble during release (bottom) for 200 ppm PAC flow.

time of release is also shown in figure 10 (bottom) where the pressure decreases to approximately 300mbar. Pressures were recorded for approximately 80s. Although the same trend as seen in figure 3 and figure 5 is seen from figure 10, it is clear that the small bubbles in the wake of the Taylor bubble remains for a quite a long long time in PAC fluids. This is reflected as a longer relaxation time before the differential pressures converge back to zero.

PIV analysis of the falling film is very difficult with the present setup, due to lack of an optical correction box. The intense light reflection of the laser sheet in the bubble as well as in the pipe was very disturbing for the analysis. Although processing the images using grey scale and histogram processing, the appearance of these disturbances were still present. However, analyzing the high speed images frame by frame, it is possible to identify the position and velocity of a seeding particle that follow the bubble film as a function of time. The result from such analysis is presented

in figure 11. This plot was produced by

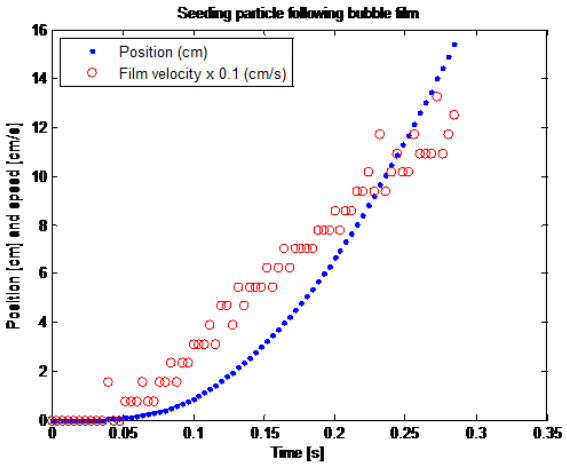

Figure 11: The position and speed (circled) of seeding particles following the falling film in 400 ppm PAC flow.

tracking the particles from approximately 70 frames. The slug bubble velocity using high speed images was measured to be 31.5 cm/s which essentially matches the calculated velocity from the ΔP data. The seeding particles are small and nearly immobile in the PAC fluid above the Taylor bubble until they are reached by the bubble nose. It can be seen from figure 11 that the film velocity accelerates from its minimum, i.e. just above the bubble, until close to position 9.5 cm, i.e. when the bubble has passed the field of view. The velocities are calculated as the time derivative of the particle positions. The development of the falling film from nose to tail is consistent with Sousa *et al.*[1,2,5] and with Bugg and Saad[10]. It is in principle possible to calculate the thickness of the film surrounding the Taylor bubble at any position based on the local film velocity. The procedure is based on tracking selected seeding particles that follow the averaged film velocity - a method still under development. A preliminary analysis of some particles in 400 ppm PAC flows indicates a ratio of terminal film thickness to pipe radius equal to 0.14. Published data from Bugg and Saad[10] for water indicate a value of 0.24.

CONCLUSIONS

A flow rig for studying Taylor bubble dynamics propagating through a vertical tube has been constructed and used for the tests. The focus has been to study various section of the bubble pattern, in particular the nose and tail regions.

The velocity of the bubble was measured both using PIV and by sets of differential pressures.

The prediction of the rise velocity of the bubble was in good agreement with the results from ΔP measurements. Tests indicate that the main effect of a sudden pressure release is that the Taylor bubble experiences a fast initial expansion leading to a liquid level rise in the pipe. This stage is then followed by a stabilized flow as in traditional stagnant liquid situations. The time required for stabilization depend on the liquid column height, and is associated with the time it takes to accelerate the liquid.

200 and 400 ppm of PAC dissolved in water have been used for demonstrating the effect of non-Newtonian fluid. The non-Newtonian fluids used for the tests are shear thinning. Generally, high viscosity fluids give more stable bottom region of the Taylor bubble, i.e flat edge, than water. This also causes less bubble production in the wake behind the Taylor bubble. On the other hand, the shear thinning property forces the smaller bubbles to remain in the wake for much longer time than for water. An interesting question from these two opposing trends then arises as to what rheology causes the least - or alternatively most bubbles - in the bubble wake. This may have important impact on fluid fraction and pressure profiles with relevance also to industrial applications. In this connection also quickly expanding bubbles behave differently, since the wake is initially much more irregular.

ACKNOWLEDGEMENTS

The work was carried out at the Two

Phase Flow Laboratory at the University of Stavanger, Norway. Thanks are given to Svein Myhren for his valuable help in the signal instrumentations. The instrumentation for this work, laser and high-speed camera was granted from the Norwegian Research Council.

REFERENCES

1. Sousa, R.G., Riethmuller, M.L., Pinto, A.M.F.R., Campos, J.B.L.M (2006), "Flow Around Individual Taylor Bubbles Rising in Stagnant Polyacrylamide (PAA) Solutions." J. Non-Newtonian Fluid Mech. 135, 16-31.

2. Sousa, R.G., Riethmuller, M.L., Pinto, A.M.F.R., Campos, J.B.L.M (2005), "Flow Around Individual Taylor Bubbles Rising in Stagnant CMC Solutions: PIV Measurements." Chemical Engineering Science, 60, pp. 1859-1873.

3. Das, G., Das, P.K., Purohit, N.K., Mitra, A.K. (1998), "Rise Velocity of a Taylor Bubble Through Concentric Annulus." Chemical Engineering Science, 53,No. 5, pp. 977-993.

4. Viana, F., Pardo, R., Yánez, R., Trallero, J.L., Joseph, D.D., (2003), "Universal Correlation for the Rise Velocity of Long Gas Bubbles in Round Pipes." J. Fluid Mech, Vol. 494, pp. 379-398.

5. Sousa, R.G., Pinto, A.M.F.R., Campos, J.B.L.M (2007), "Interaction between Taylor bubbles Rising in Stagnant non-Newtonian Fluids." International Journal of Multiphase Flow, 33, pp. 970-986.

6. Rabenjafimanantsoa, A.H., Time, R. and Saasen A. (2007), "Characteristic of the velocity profiles over fixed dunes in pipe", Annual Transactions of the Nordic Rheology Society, Vol. 14, 141-147.

7. DynamicStudio software version 2.10.86, DantecDynamics A/S

8. Sveen, J.K. (2004), "An Introduction to MatPIV." Version 1.6.1. Eprint No. 2, ISSN 0809-4403, Department of Mathematics, University of Oslo. http://www.math.uio.no/∼ jks/matpiv.

9. Rabenjafimanantsoa, A.H. (2007), "Particle Transport and Dynamics in Turbulent Newtonian and non-Newtonian Fluids." PhD Thesis No. 36, ISBN 978-82-7644-323-3. University of Stavanger, Norway.

10. Bugg, J.D. and Saad, G.A (2002), "The Velocity Field Around a Taylor Bubble Rising in a Stagnant Viscous Fluid: Numerical and Experimental Results." International Journal of Multiphase Flow, 28, pp. 791-803.